Charge transfer characterization of ALD-grown TiO_2 protective layers in silicon photocathodes

Carles Ros[a,*], *Teresa Andreu*[a,b,*], *María Dolores Hernández-Alonso*[c], *Germán Penelas-Pérez*[c], *Jordi Arbiol*[d,e], *Joan R. Morante*[a,b]

[a] Catalonia Institute for Energy Research (IREC). Jardins de les Dones de Negre 1, 08930 Sant Adrià del Besòs, Barcelona, Spain

[b] Universitat de Barcelona (UB), Martí i Franquès, 1, 08028 Barcelona, Spain

[c] Repsol Technology Center, Agustín de Betancourt, s/n, 28935 Móstoles, Madrid, Spain.

[d]Catalan Institute of Nanoscience and Nanotechnology (ICN2), CSIC and The Barcelona Institute of Science and Technology (BIST), Campus UAB, Bellaterra, 08193 Barcelona, Spain

[e]ICREA, Pg. Lluís Companys 23, 08010 Barcelona, Spain

KEYWORDS

PEC cells; silicon; protecting overlayers; water splitting; solar hydrogen production; titanium dioxide; atomic layer deposition

ABSTRACT

A critical parameter for the implementation of standard high-efficiency photovoltaic absorber materials for photoelectrochemical (PEC) water splitting is its proper protection from chemical corrosion while remaining transparent and highly conductive. Atomic layer deposited (ALD) TiO_2 layers fulfill material requirements while conformally protecting the underlying photoabsorber. Nanoscale conductivity of ALD TiO_2 protective layers on silicon based photocathodes has been analyzed, proving that the conduction path is through the columnar crystalline structure of TiO_2. Deposition temperature has been explored from 100 to 300 ºC, and a temperature threshold is found to be mandatory for an efficient charge transfer, as a consequence of layer crystallization between 100 and 200 ºC. Completely crystallized TiO_2 is demonstrated to be mandatory for long term stability, as seen in the 300 h continuous operation test.

1. INTRODUCTION

As society faces the problems derived from global warming, harvesting solar energy and storing it into chemical bonds is one of the most promising paths in the so called solar fuels economy[1] combined with the introduction of renewable energies. Between them, photoelectrochemical (PEC) water splitting offers the possibility to directly convert water and solar energy into hydrogen and oxygen with competitive efficiencies[2]. Estimating the actual photovoltaic conversion efficiency and the current commercial electrolyzer yield, the direct conversion of solar energy into chemical one (solar-to-hydrogen, STH), starts to be competitive above 10%[3].

Although this technology has been known for decades[4], still many of the published values show conversion efficiencies too low, and only few long term durability tests have been reported up to now. Combining efficiency and stability, while being cost effective, is the most relevant challenge to overcome.

During the last years, many works have been focused on understand the capacity of different non expensive metal oxides materials such as TiO_2[5], WO_3[6], $BiVO_4$[7] or Fe_2O_3[8] or oxynitrites such as TaO_xN_y[9] with band gaps large enough to split the water molecule but still able of harvesting a significant portion of the solar spectra, all of them being photoanodes due to their n-type semiconductor type[5,10–13]. In parallel, many standard electronic semiconductor materials such as Si, GaAs, CdTe or chalcogenides[14,15], have also been explored as electrode materials with high photon absorption coefficients for tandem configurations[16], although with many electrochemical stability limitations which have required different protection and surface catalyst coating strategies. Many of these semiconductors are well known from the photovoltaic or microelectronic industry, being silicon the most commercially developed due to its performance and abundance. Nevertheless, silicon, like other standard electronic semiconductors, when exposed to acidic electrolytes has a high surface oxidation rate, limiting its long term electrochemical performance[17,18]. To enable silicon to be used as front illuminated photocathode for long term hydrogen evolution, transparent, protective and conductive coatings are required[19]. Coatings must be stable in aqueous electrolytes, transparent to solar spectra to maximize photon absorption and to have a proper band alignment to facilitate minority carrier injection[20–22].

One of the proposed coating candidates is titanium dioxide (TiO_2), as it is known to be stable in a wide range of pH[23,24]. Also, TiO_2 has 3 eV band gap for rutile and 3.2 eV for anatase crystalline structure, allowing excellent optical transmittance, making TiO_2 an excellent

candidate as photocathodes protection layer[25,26]. In the case of photoanodes, ultrathin (2 nm) TiO_2 has been used to protect them for some hours while conducting by tunneling[27] and recently, thanks to an electronically "leaky" behavior, over 100 nm thick TiO_2 layers were reported conductive and stable for over 100 h by the Lewis group even though a large valence band offset between the Si and TiO_2, attributed to Ti^{3+} related mid-band states closely aligned with the Si valence band [28–31], although there is some controversy on the conduction mechanism[32]. In the case of photocathodes, it should be taken in account that TiO_2 has n-type semiconductor electrical characteristics due to oxygen vacancies, with its conduction band energetic level almost aligned with the silicon photoabsorber material for an efficient electron transport towards the electrolyte interface for hydrogen evolution reaction (HER).In this context, other works have deposited TiO_2 by sputtering and some via atomic layer deposition (ALD), all of them requiring further post-annealing process at least at 400 ºC for relevant stability[33] . ALD has attracted much attention during the last decade as it allows depositing thin and conformal layers with minimal pinholes, and recently this technique has been upgraded to industrial production. In spite of these powerful capabilities there are only few studies about the characteristics of ALD-grown TiO_2 for photocathodic hydrogen evolution[34,35]. Recently, we have demonstrated the feasibility of using ALD for the fabrication of photocathodes using a CIGSe chalcopyrite absorber[36], where it was proved that, in order to attain a high Solar-to-Hydrogen (STH) conversion, optimizing charge transfer processes is required. Although some other works have also used ALD-grown TiO_2, a better understanding on the growth process and evaluation of the final TiO_2 properties as transparent, protective and conductive layer is needed. The growth of TiO_2 by ALD is known to produce amorphous or crystalline phases depending on temperature, precursors, impurities, substrate material or film thickness[37], and hence the charge transfer

characteristics from the absorber silicon to the electrolyte through this layer become function of its deposition parameters.

To the best of our knowledge, there are not detailed microscopic analysis about the influence of electrical characteristics and deposition conditions of ALD coating layers on the final photoelectrochemical characteristics of TiO_2 protected photocathodes. Among them, temperature is one of the critical factors, being ALD crystallization temperature normally lower than those reported for post-annealing processes thanks to surface mobility of intermediate reaction species[38,39]. Reducing process temperature while maintaining optimal properties is highly interesting to decrease fabrication costs and to enable novel photoabsorbing materials sensible to temperature[40].

On the other hand, one of the main concerns is relative to the internal interface between silicon and the coated layer. Si native oxidation forms a narrow SiO_x layer. In previous works, controlled SiO_x has been used to maximize the photovoltage thanks to the creation of a MIS junction[41,42], but in our case the photovoltage is created by the buried n^+-p silicon junction. To avoid SiO_x being formed, which in our case would act as a series resistance, a thin metallic titanium layer is deposited on the cleaned silicon surface before the TiO_2 deposition to inhibit ambient or ALD-process[42] oxidation of Si, assuming a small light shielding of the metallic film, and by HRTEM it is confirmed that no SiO_x is formed. $TiCl_4$ has been selected as the precursor material thanks to its wide deposition range[38] compared to other precursors known for ALD-TiO_2[43].

In the present study, in order to understand the role of the crystallographic structure on the charge transfer across these coated layers and its stability, TiO_2 layers have been grown by ALD at different deposition temperatures on different silicon based substrates using $TiCl_4$ as

precursor. The growth temperature has been modified from 100ºC to 300ºC and a model is presented to explain the charge transfer mechanism across the ALD layer.

2. EXPERIMENTAL

ALD TiO_2 has been grown on n^+-p silicon buried junctions and simultaneously on n^+ degenerately doped silicon, to simulate direct injection in dark conditions.

n^+-Si samples were created by cutting in 1x1 cm^2 pieces a degenerately doped silicon wafer (0.001 ohm·cm), and 50 nm Al were thermally evaporated as back contact. To prevent the formation of any native SiO_2 and avoid its potential negative effects, in some of these samples, 5 nm Ti were thermally evaporated on top of it (Ti/n^+-Si). Titanium thickness was controlled by a quartz microbalance.

For the Ti/n^+p-Si samples, a 1 cm^2 active area was lithographically defined by SiO_2 passivation on a silicon p-type wafer (0.1-0.5 ohm.cm resistivity). Boron was implanted in the defined front surface and activated by rapid thermal annealing, creating a 200 nm n^+ region on top of the p-type substrate. Sample's front surface was dipped in HF and immediately coated with 5 nm Ti by sputtering. As back contact, 1 μm Al/0.5%Cu was sputtered on top of 30 nm Ti to form a proper ohmic contact.

n^+-Si, Ti/n^+-Si and Ti/n^+p-Si samples were sonicated for 5 min in a 1:1:1 isopropanol, acetone and DI water cleaning solution, followed by abundant rinsing and further 5 min sonication in DI water. Samples were simultaneously introduced in a R200 Picosun Atomic Layer Deposition system. $TiCl_4$ was selected as precursor due to its wide temperature stability range. $TiCl_4$ and H_2O precursors at 19 ºC were used in successive pulses at 8 mbar in N_2 flow atmosphere, with 0.1 s pulses and 10 s purges. Under these conditions, layers have been grown at deposition

temperatures of 100, 200 and 300 ºC for 3700 cycles, corresponding to roughly 100 nm layers for 200 ºC. Layer thickness was measured by evaluating the reflected spectra with a Sensofar interferometer device with ± 0.2 nm error. Finally, platinum was deposited either by thermal evaporation (corresponding to 1 nm measured by a quartz microbalance) or 50 µl drop casting of 6.5 mM H_2PtCl_6 in isopropanol. Samples were then soldered to a Cu wire using Ag paint and epoxy protected leaving the front area exposed. For I-V measurements, 100 nm Au was thermally evaporated on TiO_2/Ti/n^+-Si samples with a circular mask 0.55 cm in diameter.

Surface and cross section morphology was observed with a Zeiss Series Auriga Field Effect Scanning Electron Microscope (FESEM). Structural characterization was carried out by X-ray diffraction (XRD) in a D8 Advance Bruker equipment with a Cu Kα radiation source working at 40 kV and 40 mA with a 3 º offset angle. Crystalline domains are calculated following the Scherrer equation: $D = 0.9 * \lambda / (\beta * \cos \theta)$, where λ is the X-ray wavelength (1.5406 Å), β is the full width of the diffraction line at half maximum (FWHM), and β is the Bragg angle. High resolution transmission electron microscopy (HRTEM), high angle annular dark field (HAADF) scanning TEM (STEM) and electron energy loss spectroscopy (EELS) spectrum imaging (SI) were performed using a TECNAI F20 operated at 200 kV with a point to point resolution of 0.14 nm. AFM and Conductivity-AFM measures were taken with a Park Systems XE-100 with platinum conductive cantilevers. Due to the n^+p-Si built-in voltage, only the samples on n^+-Si substrates were measured by Conductivity-AFM. The photoelectrochemical measurements were obtained with a Princeton Applied Research PARSTAT 2273 potentiostat using Ag/AgCl/KCl (3M) ($E^0 = 0.203\ V_{RHE}$) as reference electrode and platinum mesh as counter electrode. A quartz cell with flat faces was used with 100 ml of 0.5 M H_2SO_4 electrolyte and a 300 W xenon lamp

with an AM 1.5G filter under the appropriate distance to receive 100 mW/cm^2, calibrated using a silicon diode (Gentec-EO, XLPF12-3S-H2-DO).

The half-cell solar-to-hydrogen efficiency (HC-STH) was calculated from the linear sweep voltammograms using the equation HC-STH = $|j_{ph}| \times (E_{RHE}-E_{H+/H2}) / P_{sun} \times 100$ %, where j_{ph} is the photocurrent density obtained under an applied bias of E_{RHE}, $E_{H+/H2}$ is the equilibrium redox potential of hydrogen (0 V_{RHE}) and P_{sun} is the power density of the incident solar energy (100 mW·cm^{-2}). I-V curves were obtained with the potentiostat, connecting the working electrode on the back contact and the counter and reference electrodes on the top Au contact. Photoelectrochemical fill factor (FF) was defined equivalently as in photovoltaics assuming the onset potential as open circuit voltage and the current density at 0 V_{RHE} as short circuit current.

3. RESULTS AND DISCUSSION

3.1. Electrochemical characterization

In order to optimize the charge transfer process of a n^+p-Si photocathode, it is needed to consider that the electron injection will be from the doped n^+-Si to the electrocatalyst through the protective TiO_2 layer. Then, to avoid the resistive effect of the diode under dark conditions, degenerately doped n^+ 0.001 ohm.cm Si substrates has been used instead of illuminating n^+p-Si junctions, being some of them protected with Ti.

n^+-Si and Ti/n^+-Si substrates with a nominal 100 nm TiO_2 grown at different temperatures were tested as electrodes for hydrogen evolution using Pt as electrocatalyst in sulfuric acid media (0.5 M H_2SO_4) in a 3 electrodes configuration. The overall current obtained under polarization is influenced by the intrinsic conductivity of the TiO_2 and possible extra SiO_2 interlayer and also the surface charge transfer rate, which is assumed to be constant, as the HER deposited catalyst

is the same. Thus, any variation in the measured current is attributable to the TiO_2 or the presence of a resistive SiO_2 interlayer. As seen in Figure 1, polarization curves show a clear influence of ALD deposition temperature. Regardless of the titanium layer presence, the current density reached at the same polarization is higher as the growth temperature increases. Comparing the results obtained with both substrates, n^+-Si and Ti/n^+-Si, it can be observed that, under the same experimental conditions, higher current densities were obtained in samples where the TiO_2 layer was grown on Ti/n^+-Si. On bare n^+-Si, the presence of a native SiO_2 layer is expected, introducing significant resistance to the system, lowering the obtained electrochemical current. This native layer can be thus avoided with the metallic 5 nm Ti layer.

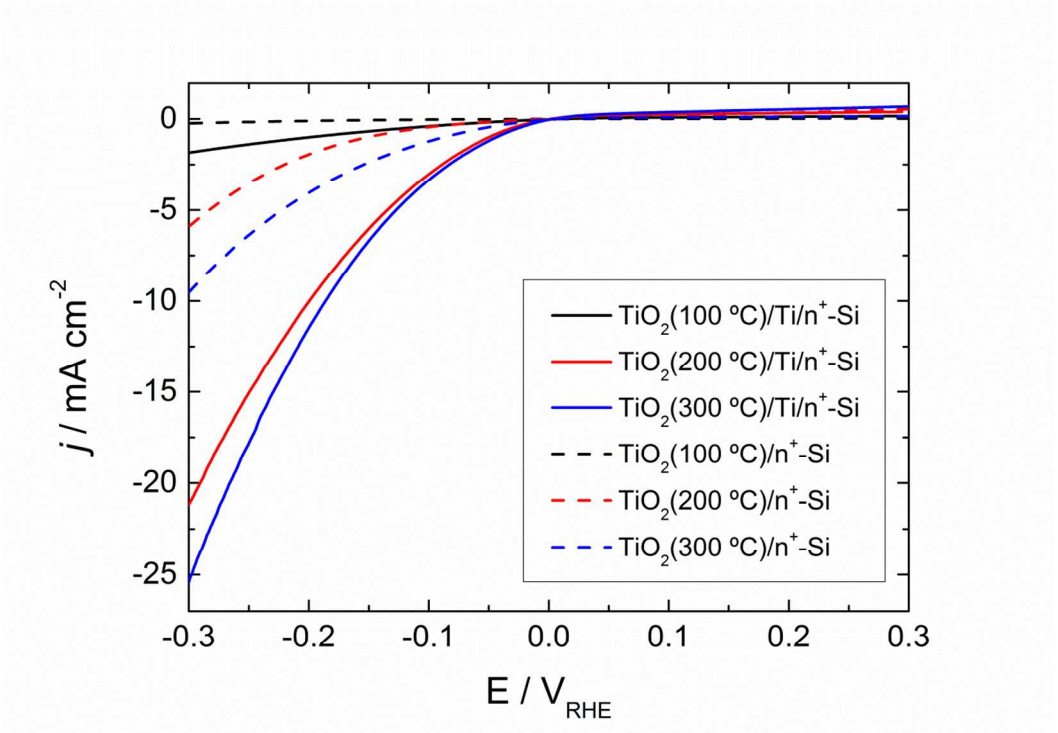

Figure 1. Polarization curves of TiO_2 layers grown at different temperatures on Ti/n^+-Si substrates (solid lines) and n^+-Si (dotted lines) ranging from 100 to 300 ºC. 1 nm Pt was evaporated on top as HER catalyst. Measurements were made in 0.5 M H_2SO_4 with Ag/AgCl as reference electrode and Pt as counter in 3 electrodes configuration with no illumination.

3.2. Morphological and structural characterization

No visible pinholes have been detected by direct analysis of the SEM images of the TiO_2 layers grown by ALD (Figure 2 a-c) on Ti/n^+-Si substrates. Increasing temperature from 100 to 300 ºC shows remarkable variation in the film topography, which is proven by XRD to correspond to TiO_2 crystalline growth, starting between 100 and 200 ºC and presenting anatase structure. The deposition temperature range was set up to 300 ºC to obtain complete layer crystallization on all substrates.

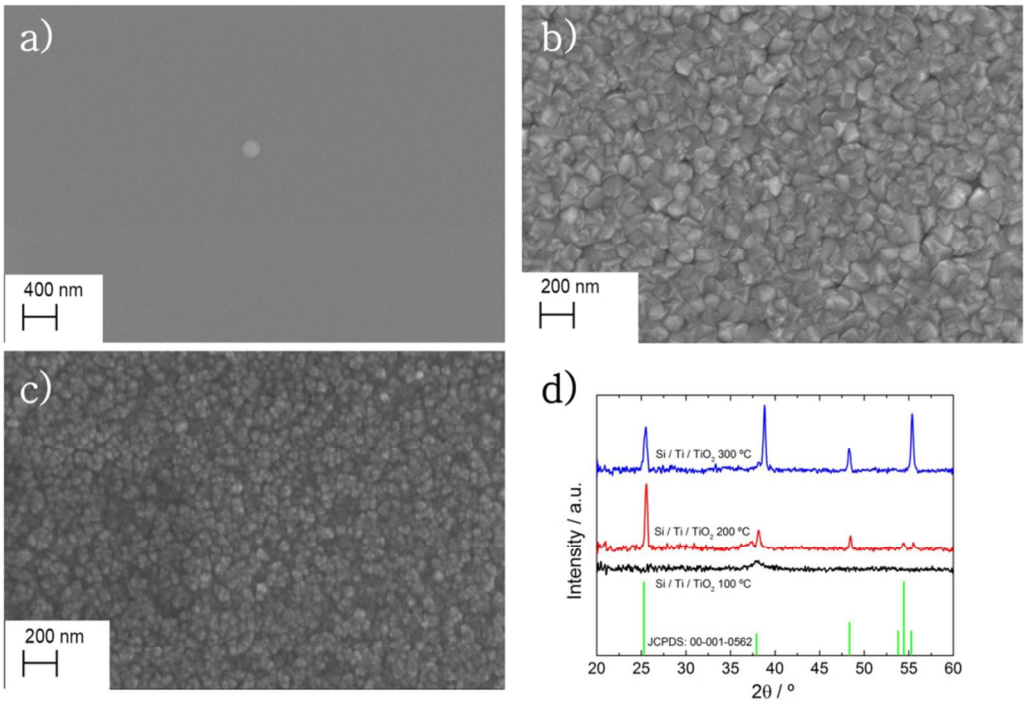

Figure 2. SEM images of TiO_2 layers grown by 3700 ALD cycles of $TiCl_4$ and H_2O on Ti/n^+-Si substrates at a) 100 ºC, b) 200 ºC and c) 300 ºC. d) XRD patterns of TiO_2 layers grown on Ti/n^+-Si substrates at 100 ºC, 200 ºC and 300 ºC.

For ALD layers deposited on Ti/n^+-Si substrates, XRD shows that at 100 ºC amorphous layers are grown, while anatase TiO_2 is obtained at 200 and 300 ºC (Figure 2.d). This is in agreement with electrochemical charge transfer shown in Figure 1, with amorphous layers inhibiting charge transfer, meanwhile crystallization enables current flow, and more stable TiO_2 phases further reduce electrical resistance. Preferential growth direction with the 25.5 º peak is shown at 200 ºC but not at 300 ºC, as higher nucleation rate inhibits preferential directions to develop[44]. This phase transition is in accordance with other studies[38].

Samples without the intermediate Ti layer (where Si was exposed to air, creating a native SiO_2 layer) show the same behavior but shifted to higher temperatures (Figure S.2 a-c), with 300 ºC grown samples still showing preferential growth directions (Figure S.3).

Crystal nucleation is favored as temperature increases, starting at a temperature higher than 100 ºC as seen in SEM. At 200 ºC, grains ranging 180 nm in diameter can be seen on n^+-Si substrates, whereas less than 20 nm diameter ones can be seen at 300 ºC on Ti/n^+-Si, with a higher grain density and size dispersion due to increased nucleation and competiveness. Higher thermal energy enhances nucleation kinetics by overcoming its activation energy, favoring nucleation in front of growth and resulting in more and smaller grains. Increasing temperature is also expected to improve atomic order in the crystal structure. From XRD data and using the Scherrer equation, the mean size of the crystalline domains has been calculated. Sizes of 33.2 nm for 200 ºC and 25.9 nm at 300 ºC on n^+-Si, and 26.3 and 22.2 nm for 200 and 300 ºC on Ti/n^+-Si substrates have been obtained. Calculated crystallite size suggests that multiple crystallographic domains are present in the same observable grain. Crystal size is reduced when deposition temperature increases, as it is expected for higher nucleation.

Layer thickness is also dependent on the crystallographic phase. As can be seen in the cross section SEM image (Figure 3), grains are thicker than the amorphous layer. We should expect thinner layers where they crystalize into more compact phases, as far as the amount of precursor is kept constant. However, anatase phase is more favorable to OH^- adsorption, and higher superficial OH^- density increases the growth per cycle by a higher ALD reactivity, thus generating thicker layers where there is a crystallized zone[43].

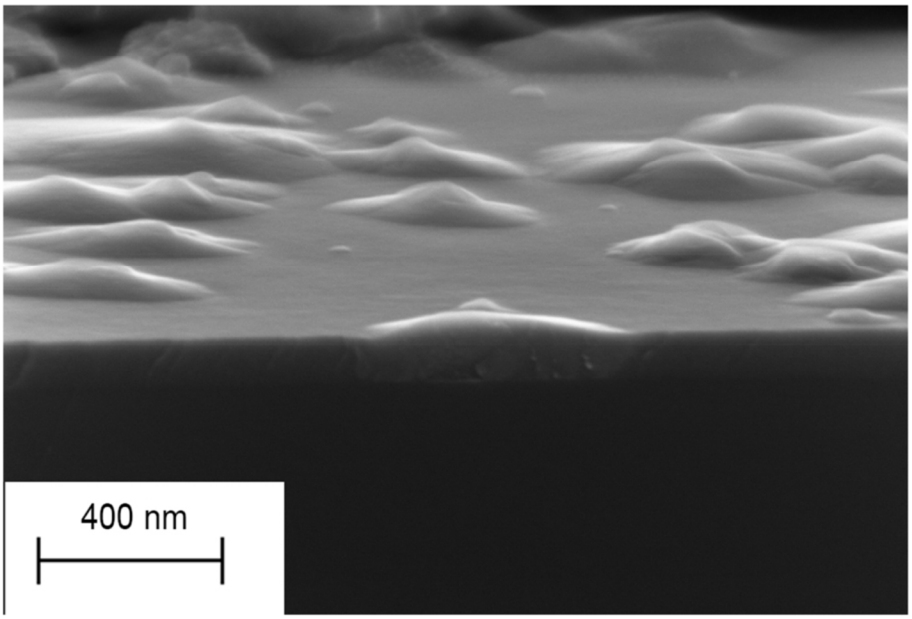

Figure 3. Cross section SEM image of a 3700 cycles TiO_2 layer on n^+-Si grown at 200 ºC

As seen in the HRTEM cross section (Figure 4) of a processed Ti/n^+p-Si sample, a native 3.5 nm TiO_x overlayer is formed on metallic Ti when exposed to air. This layer seems to enhance nucleation and so, due to growth competition amongst different grains, reduction of crystallite size by crystal overlapping takes place. Lower lattice mismatch is the cause of enhanced nucleation on TiO_2/Ti substrates compared to SiO_2/Si, leading to crystallization temperature

reduction, as TiO_2 is known to start growing in amorphous phase for the initial ALD cycles[38]. By AFM it was discarded to be caused by higher substrate rugosity (Figure S.4).

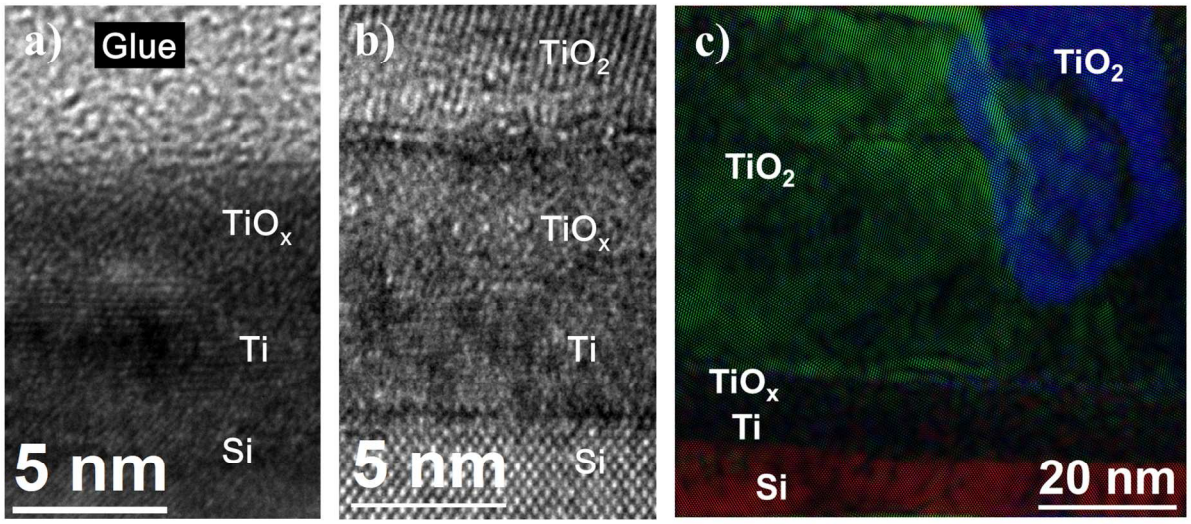

Figure 4. HRTEM images of a Ti/n^+p-Si substrate a) prior to ALD deposition b) with 3700 ALD cycles of TiO_2 grown at 200 ºC. c) Reciprocal space phase filtered HRTEM image composition. Crystals starting on the native TiO_2 and propagating vertically in a columnar configuration can be seen.

From the HRTEM image of TiO_2 on Ti/n^+p-Si, it is confirmed that the presented ALD crystal has anatase crystallographic phase (Figure 4). The observed metallic Ti on silicon is 5 nm thick, and its native TiO_2 layer is 3.5 nm. Ti presents polycrystalline structure with preferential {10-10} planes parallel to the (001) Si substrate. The native layer is amorphous, as the 200 ºC annealing caused by the ALD deposition process is not enough to crystallize it. EELS TEM imaging (Figure S.5) confirms progressive reduction of the oxygen content in the native layer, with 5 nm metallic Ti remaining after ambient exposition during laboratory manipulation and processing,

proving it is thick enough to act as oxidation barrier avoiding oxygen diffusion towards the Si photoabsorber. This 5 nm Ti layer is expected to partially block light from reaching the Si, and thus significantly reducing the photon to current conversion efficiency.

It is important to note that the bottom part of the ALD layer was crystalline, meaning nucleated crystals not only propagate upwards, but also laterally[45]. The substoichiometry of the native oxide layer must prevent its recrystallization. Reciprocal space phase filtered HRTEM presents columnar epitaxial growth from the base to the top of the ALD layer (Figure 4).

3.3. Solid state electrical characterization

A conductivity AFM was used to visualize the conduction path across the TiO_2 layer, similarly to the measurements performed by Wang's group on hematite[46]. From the topography image of a sample grown at 200 ºC on bare n^+-Si substrates (Figure 5.a), we can see that successive ALD deposition formed isolated grains, as seen in SEM (Figure 3). From conductive measurements (Figure 5.b), it is perfectly seen that the whole grain structure is the path for the current flow, with similar current intensities at a fixed voltage. Comparing topography and conductivity AFM measurements, and as suggested by Scherrer equation, multiple crystallite boundaries can be seen in each grain as more resistive regions. No current is detected from the amorphous regions, as atomic disorder gives significantly reduced electron mobility and larger resistance than crystalline TiO_2. From a sample grown at 300 ºC on Ti/n^+-Si (Figure 5.c,d), where no amorphous phase is present, similar current intensity is detected from all grains. Also, grain boundaries are much less conductive.

Columnar grain growth together with conductivity through the crystalline grains is the key for a good electrical transport from the photoabsorbing material to the catalyst to perform the

hydrogen evolution reaction. No grain boundaries are seen by HRTEM in the vertical direction, being those one of the main electron mobility barriers for polycrystalline conductive materials. Increasing deposition temperature increases the number of grain boundaries in the lateral but not in the vertical direction, and also enhances crystallographic order, a parameter for higher electron mobility. This is in accordance with obtaining higher conductivity in the samples grown at higher temperature.

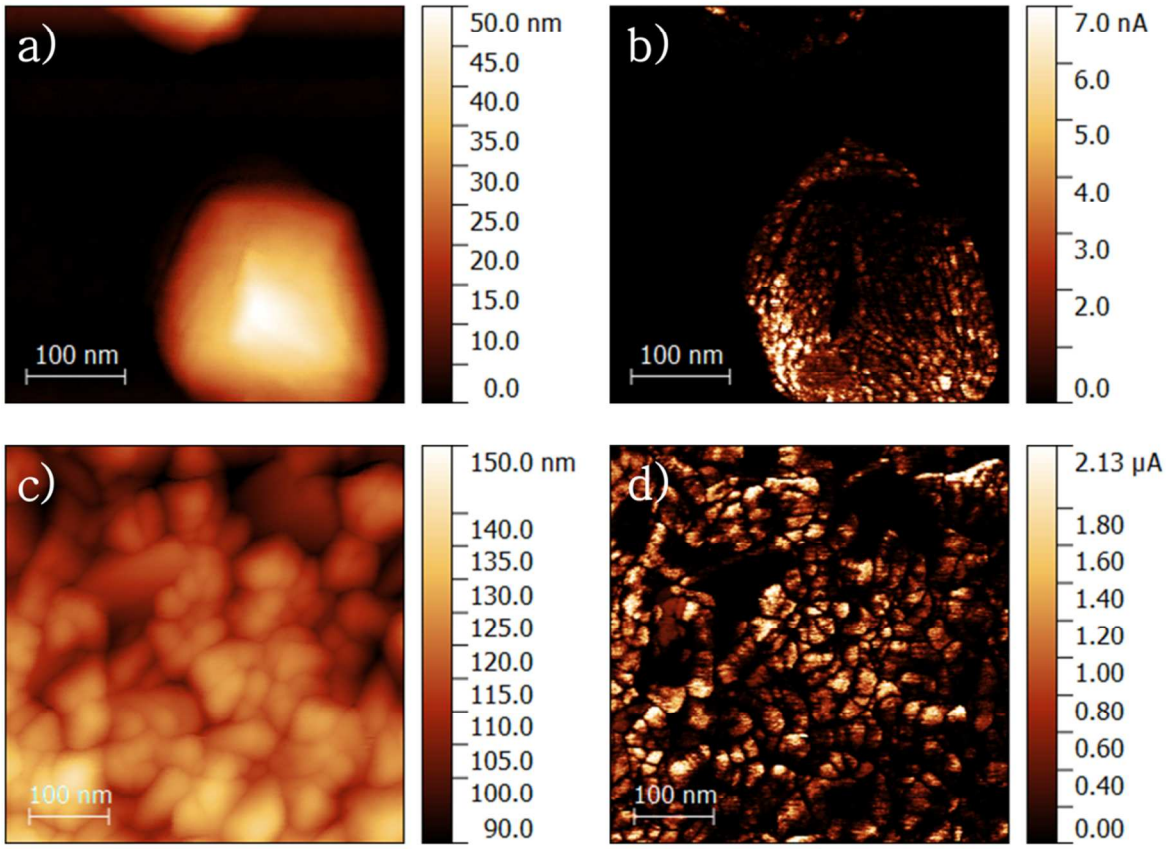

Figure 5. AFM and c-AFM images of TiO_2 ALD layers on an n^+-Si substrate. a) Height map of a sample grown at 200 ºC, b) current intensity image of the same sample. c) Height map of a sample grown at 300 ºC and d) its current intensity map.

To deeply analyze and quantify the conduction across ALD-grown TiO_2 layers on Ti/n^+-Si, 100 nm of Au were deposited by thermal evaporation to form a top, highly conductive and defined contact (Figure 6.a). As seen in Figure 6.b, a nonlinear behavior and higher currents for negative polarization can be distinguished, meaning that our system presents a rectifying behavior: a Schottky barrier junction, formed between the TiO_2 and the Au top contact. The degenerately doped n^+-Si/Ti junction and the progressive interface between Ti and TiO_2 (due to the oxygen chemical affinity of Ti) form ohmic-like contacts, injecting electrons from the n^+-Si conduction band into the TiO_2 conduction band[47]. The conductivity increment with higher ALD growth temperatures is clearly shown, presenting the same trend determined by previous electrochemical measurements (Figure. 1).

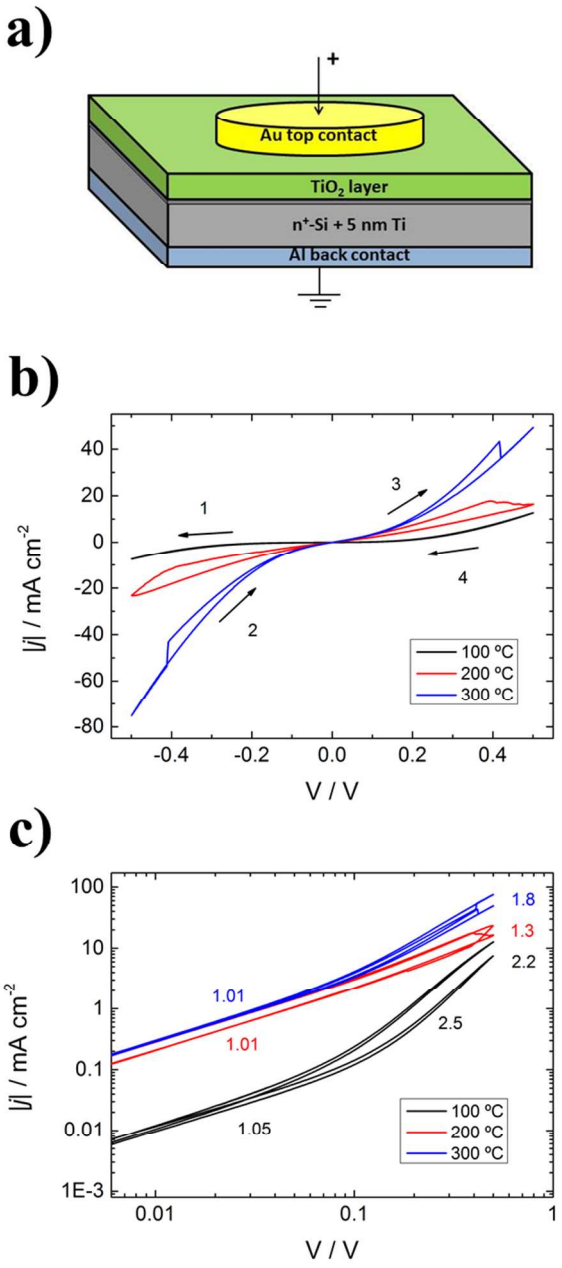

Figure 6. a) Scheme of the stack. b) I-V c) log-log curves of the Au top-contacted TiO_2 layers grown at 100 ºC (black), 200 ºC (red) and 300 ºC (blue). Numbered arrows show the direction of the polarization curve in b) and the slope in c) is indicated for each different segment of the log-log graph. Measurements were recorded at 50 mV/s.

Samples grown at 200 and 300 ºC present a reversible switch between a high resistivity (HR) and a low resistivity (LR) state. Anatase-crystallized TiO_2 is known to behave as n-type semiconductor due to oxygen vacancies, regarded to be fully ionized even at room temperatures, giving free electrons to act as charge carriers. These changes while cycling have been explained by some papers during the last decade [47–51], and are attributed to ionic diffusion of the oxygen atoms due to polarization, leaving extra free charges (oxygen vacancies) which enhance the electronic conductivity[47]. Current flow through defects on the crystallographic structure can create local heating, enhancing ionic diffusion, and forming highly conductive paths or filaments, giving the LR state. Reversing the polarization returns the oxygen ions, destroying the filaments, and resetting the sample to the HR state. The sample grown at 300 ºC has an almost immediate change in the resistivity state, while the sample fabricated at 200 ºC has a more progressive one. This difference could be justified by the poor crystallographic quality at 200 ºC, lowering the ionic mobility together with a general lower conductivity, which gives less local heating.

From the log-log plot (Figure 6.c), an ohmic dependence ($I \alpha V$) is observed for all samples on small polarization potentials. Further increasing the potential, slope increases for all samples. This behavior fits to a space charge limited (SCL) conduction mechanism ($I \alpha V^2$)[52] together with the Au/TiO_2 Schottky Barrier junction. For polarization values inside the ohmic regime, we can measure resistances from 221 $\Omega \cdot cm^2$ for the sample grown at 100 ºC, to 41 and 21 $\Omega \cdot cm^2$ for 200 and 300 ºC-grown samples. If we measure the potential drop in the layer at 5 mA/cm^2, we obtain 430 mV for 100 ºC, 213 and 151 mV for HR and LR states at 200 ºC, and 118 and 112 mV for HR and LR at 300 ºC.

3.4. Photoelectrochemical characterization

ALD-grown TiO_2 layers were used to protect n^+p-Si substrates having a thin ~5 nm Ti layer (Ti/n^+p-Si) at deposition temperatures of 100, 200 and 300 ºC. When exposed to AM 1.5G illumination, the p-n junction properly separates the electron-hole pairs, giving an onset voltage around 0.6 V vs RHE (Figure 7). More than 100 mV/dec potential losses should be expected by the electrochemical kinetics of hydrogen evolution, even when using platinum as catalyst[53].

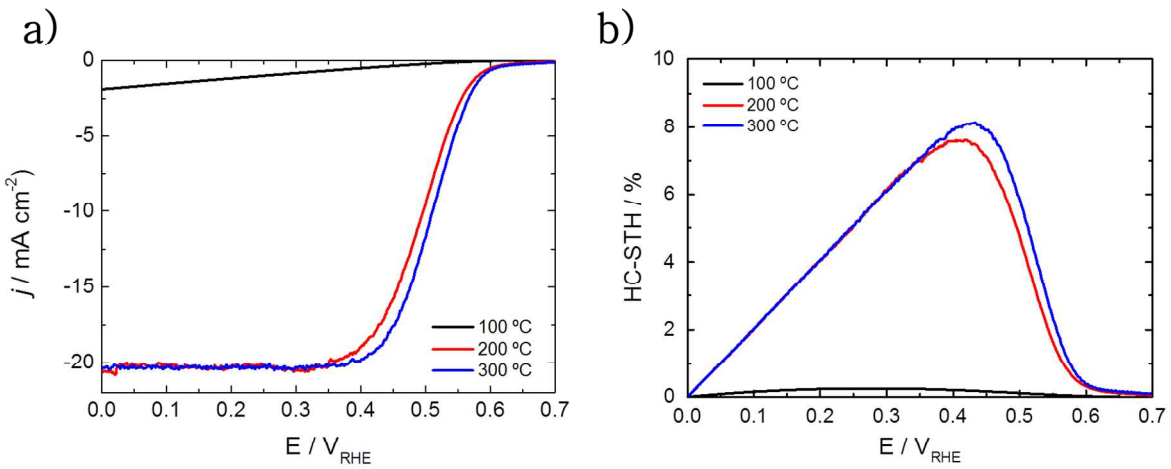

Figure 7. a) polarization curves and b) HC-STH calculations of TiO_2 layers grown at different temperatures on Ti/n^+p-Si substrates ranging from 100 to 300 ºC. 1 nm Pt was evaporated on top as HER catalyst. Measurements under 1 sun AM 1.5G illumination in 0.5 M H_2SO_4 with Ag/AgCl as reference and Pt as counter electrode in 3 electrodes configuration.

The layer growth temperature influences significantly the sample's efficiency. Samples grown at 100 ºC show a highly resistive response (with a fill factor (FF) of 0.26), meanwhile FF is significantly improved when increasing growth temperature. At 200 ºC, which corresponds to samples with polycrystalline anatase layers combined with amorphous regions, a FF of 0.66 is

obtained. At 300 ºC, the slope of the *j*-V curve is slightly increased, together with the FF, up to 0.73 (Table 1).

Table 1. Photogenerated current densities and voltages under 1-sun illumination of the samples grown at different temperatures.

Growth temperature (ºC)	***j* at $0V_{RHE}$ (mA/cm^2)**	**V_{ONSET} (V_{RHE})**	***Fill Factor***	***HC-STH* (%)**
100	1.9	0.59	0.26	0.25
200	20.6	0.63	0.66	7.60
300	20.3	0.64	0.73	8.10

This enhancement in the saturation slope is directly related to growth temperature via reduction of the deposited layer resistivity. With such improvement, a half-cell solar-to-hydrogen conversion efficiency (HC-STH) of up to 8.1 % can be reached. The effect of TiO_2 layers with different resistivity on silicon photocathodes band diagrams is schematically represented in Scheme 1. For high resistive layers, the voltage drop across the protective layer causes a decrease in the fill factor. For the more crystalline and less resistive layer, the lower voltage drop allows an optimum electron transfer. Then, the main factors contributing to the FF characteristics of the polarization curve are the buried p-n junction and the platinum HER overpotential.

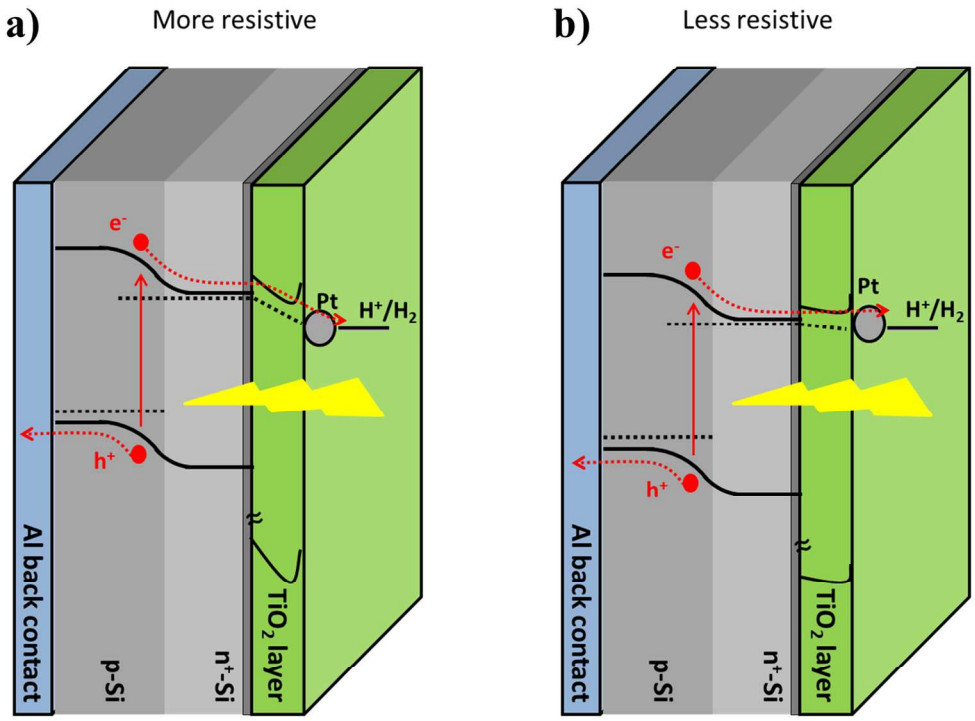

Scheme 1. Charge transfer model in working conditions with a) high resistance and b) low resistance TiO_2 layer.

Long term stability experiments were performed under 1 sun AM 1.5G illumination at 0.3 V_{RHE} in 0.5 M H_2SO_4 with n^+p-Si photocathodes protected with either an almost-completely crystalline TiO_2 layer and a fully crystalline one.

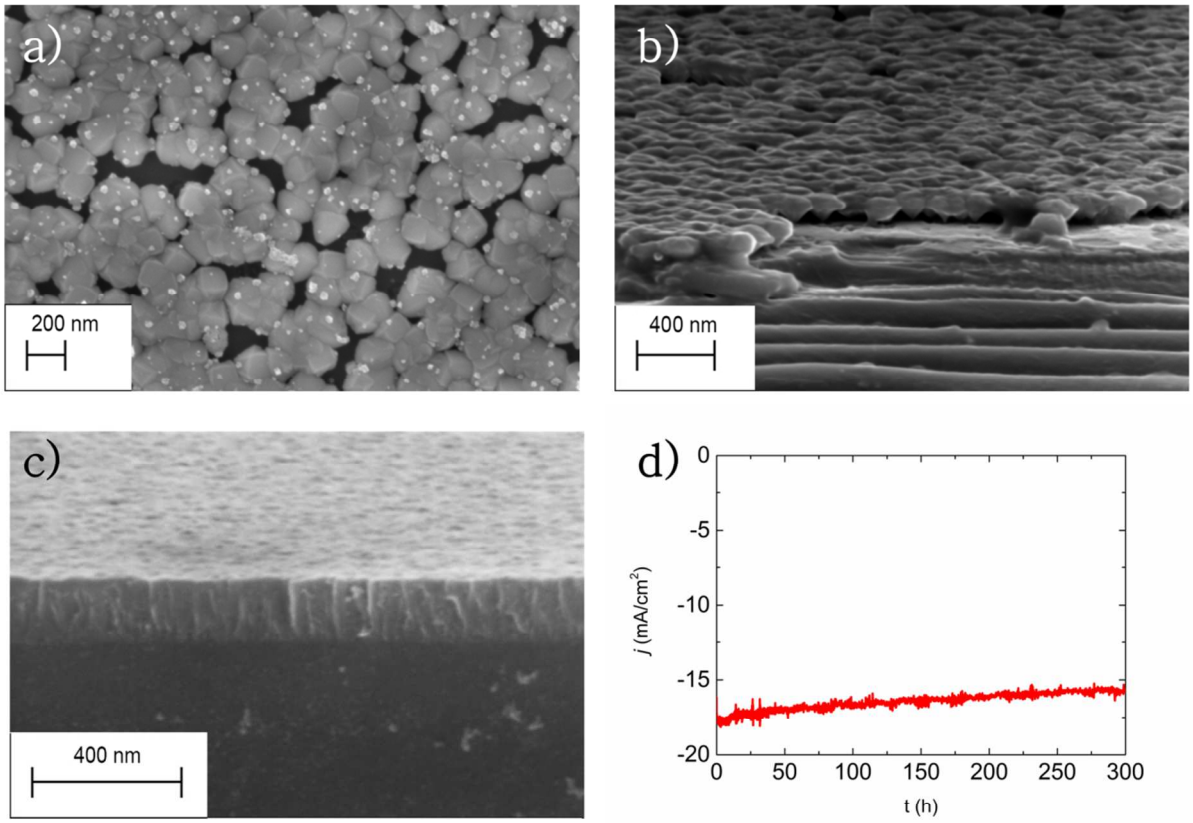

Figure 8. a) Top and b) cross section SEM images of an almost-crystalline TiO_2 layer after a stability test, where dissolution of the amorphous region between crystals can be seen. c) Cross section of a fully crystallized layer after 300 h stability in 0.5 M H_2SO_4, with no visible dissolution. d) Current measurement of the fully-crystalline TiO_2 sample for 300 h at 0.3 V_{RHE} under 1 sun AM 1.5G illumination.

After examining the almost-completely crystalline TiO_2 layer by SEM (Fig. 8a,b), we can clearly see how the top view is similar to as-grown layers (Figure 2.b), with darker zones between the crystals. Cross section SEM image evidences that those gaps are missing TiO_2. At reductive potentials and using an acidic electrolyte (0.5 M H_2SO_4), the amorphous TiO_2 phase

has dissolved, but not the anatase crystals, leaving inversed conical structures only attached to the Si by the tip. Also, silicon is not attacked, and SiO_2 is known to form, protecting the silicon from further oxidation but electrically passivating the surface. Fully crystalline TiO_2 layers present no visible dissolution, showing compact columnar crystals by cross section SEM, proving that the stability of TiO_2 shown in its Pourbaix diagram[23] is only attributable to the crystalline anatase TiO_2 crystal phase. This shows the need to use crystallized ALD layers, together with the conductivity improvement with temperature previously shown.

A stability measurement of a photocathode protected with a fully crystalline TiO_2 layer was performed for over 300 h, as shown in Figure 8.a. The sample maintained 90 % of the initial photocurrent without significant changes in the Fill Factor, as seen in Figure S.6. This slight current reduction over time has been attributed by other authors to the loss of not properly attached platinum catalyst[25,33]. To best of our knowledge, there are no reports presenting several days stability of TiO2-protected photocathodes fabricated at lower than 400 ºC.

4. CONCLUSIONS

In conclusion, we have demonstrated that the ALD growth temperature has a fundamental role on the charge transfer across protective TiO_2 coatings for front illuminated silicon photocathodes due to reduced resistivity with increasing deposition temperature. A minimum growth temperature is required for an efficient charge transfer, as a consequence of layer crystallization between 100 and 200 ºC.

From conductive AFM images, we have proven that the conduction path is through the crystalline structure of TiO_2; and that amorphous layers and grain boundaries are highly resistive. Conduction across the protective layer can be increased by using higher deposition temperatures with more stable TiO_2 phases and reducing defects and charge traps, obtaining higher fill factors

up to 0.73. The thin titanium layer used to protect silicon from oxidation has an important role also in enhancing the TiO_2 nucleation and crystallization although reducing light transmission. The formation of a TiO_x layer contributes to the nucleation of the TiO_2 ALD layer enhancing crystal density. The negative formation of a resistive SiO_x layer is avoided. Also, fully crystallized TiO_2 is demonstrated to be mandatory for long term stability, as seen in the 300 h continuous operation test.

Future studies should be addressed into achieving higher crystallization at lower temperatures, to implement ALD grown TiO_2 as protective, conductive and transparent layers for photoabsorbing materials sensible to temperature processes.

ASSOCIATED CONTENT

Supporting Information. SEM, HRTEM, XRD and AFM supplementary images, together with a photo of a finished device, are supplied in an additional document.

AUTHOR INFORMATION

Corresponding Author

*Corresponding authors:

E-mail: cros@irec.cat

E-mail: tandreu@irec.cat

Tel: (34) 933 562 615

Author Contributions

The manuscript was written through contributions of all authors. All authors have given approval to the final version of the manuscript.

Funding Sources

ACKNOWLEDGMENT

This work was supported by Repsol, S.A. Authors from IREC thank Generalitat de Catalunya for financial support through the CERCA Programme, M2E (2014SGR1638) and XaRMAE network. IREC also acknowledges additional support by the European Regional Development Funds (ERDF, FEDER) and by MINECO coordinated projects MAT2014-59961-C2 and ENE2016-80788-C5-5-R. C.R. thanks to MINECO for his FPI grant (BES-2015-071618). ICN2 acknowledges support from the Severo Ochoa Program (MINECO, Grant SEV-2013-0295).

REFERENCES

(1) Lewis, N. S.; Nocera, D. G. Powering the Planet: Chemical Challenges in Solar Energy Utilization. *Proc. Natl. Acad. Sci. U. S. A.* **2006**, *103* (43), 15729–15735.

(2) Barber, J.; Tran, P. D. From Natural to Artificial Photosynthesis. *J. R. Soc. Interface* **2013**, *10* (81), 20120984.

(3) James, B. D.; Baum, G. N.; Perez, J.; Baum, K. N. Technoeconomic Analysis of Photoelectrochemical (PEC) Hydrogen Production. **2009**, 1–128.

(4) FUJISHIMA, A.; HONDA, K. Electrochemical Photolysis of Water at a Semiconductor Electrode. *Nature* **1972**, *238* (5358), 37–38.

(5) Fàbrega, C.; Monllor-Satoca, D.; Ampudia, S.; Parra, A.; Andreu, T.; Morante, J. R.

Tuning the Fermi Level and the Kinetics of Surface States of TiO 2 Nanorods by Means of Ammonia Treatments. *J. Phys. Chem. C* **2013**, *117* (40), 20517–20524.

(6) Fàbrega, C.; Murcia-López, S.; Monllor-Satoca, D.; Prades, J. D.; Hernández-Alonso, M. D.; Penelas, G.; Morante, J. R.; Andreu, T. Efficient WO3 Photoanodes Fabricated by Pulsed Laser Deposition for Photoelectrochemical Water Splitting with High Faradaic Efficiency. *Appl. Catal. B Environ.* **2016**, *189*, 133–140.

(7) Murcia-López, S.; Fabrega, C.; Monllor-Satoca, D.; Hernández-Alonso, M. D.; Penelas-Pérez, G.; Morata, A.; Morante, J. R.; Andreu, T. Tailoring Multilayered BiVO 4 Photoanodes by Pulsed Laser Deposition for Water Splitting. *ACS Appl. Mater. Interfaces* **2016**, *8* (6), 4076–4085.

(8) Yang, X.; Liu, R.; Du, C.; Dai, P.; Zheng, Z.; Wang, D. Improving Hematite-Based Photoelectrochemical Water Splitting with Ultrathin TiO2 by Atomic Layer Deposition. *ACS Appl. Mater. Interfaces* **2014**, *6* (15), 12005–12011.

(9) Abe, R.; Higashi, M.; Domen, K. Facile Fabrication of an Efficient Oxynitride TaON Photoanode for Overall Water Splitting into H 2 and O 2 under Visible Light Irradiation. *J. Am. Chem. Soc.* **2010**, *132* (34), 11828–11829.

(10) Maeda, K.; Domen, K. Photocatalytic Water Splitting: Recent Progress and Future Challenges. *J. Phys. Chem. Lett.* **2010**, *1* (18), 2655–2661.

(11) Ni, M.; Leung, M. K. H.; Leung, D. Y. C.; Sumathy, K. A Review and Recent Developments in Photocatalytic Water-Splitting Using TiO2 for Hydrogen Production. *Renew. Sustain. Energy Rev.* **2007**, *11* (3), 401–425.

(12) Pilli, S. K.; Furtak, T. E.; Brown, L. D.; Deutsch, T. G.; Turner, J. A.; Herring, A. M. Cobalt-Phosphate (Co-Pi) Catalyst Modified Mo-Doped BiVO4 Photoelectrodes for Solar Water Oxidation. *Energy Environ. Sci.* **2011**, *4* (12), 5028–5034.

(13) Sivula, K.; Formal, F. Le; Grätzel, M. WO 3 −Fe 2 O 3 Photoanodes for Water Splitting: A Host Scaffold, Guest Absorber Approach. *Chem. Mater.* **2009**, *21* (13), 2862–2867.

(14) Wu, X. High-Efficiency Polycrystalline CdTe Thin-Film Solar Cells. *Sol. Energy* **2004**, *77* (6), 803–814.

(15) Giraldo, S.; Neuschitzer, M.; Thersleff, T.; López-Marino, S.; Sánchez, Y.; Xie, H.; Colina, M.; Placidi, M.; Pistor, P.; Izquierdo-Roca, V.; Leifer, K.; Pérez-Rodríguez, A.; Saucedo, E. Large Efficiency Improvement in Cu2ZnSnSe4 Solar Cells by Introducing a Superficial Ge Nanolayer. *Adv. Energy Mater.* **2015**, *5* (21), 1–6.

(16) Hu, S.; Xiang, C.; Haussener, S.; Berger, A. D.; Lewis, N. S. An Analysis of the Optimal Band Gaps of Light Absorbers in Integrated Tandem Photoelectrochemical Water-Splitting Systems. *Energy Environ. Sci.* **2013**, *6* (10), 2984–2993.

(17) McKone, J. R.; Warren, E. L.; Bierman, M. J.; Boettcher, S. W.; Brunschwig, B. S.; Lewis, N. S.; Gray, H. B. Evaluation of Pt, Ni, and Ni–Mo Electrocatalysts for Hydrogen Evolution on Crystalline Si Electrodes. *Energy Environ. Sci.* **2011**, *4* (9), 3573–3583.

(18) Boettcher, S. W.; Warren, E. L.; Putnam, M. C.; Santori, E. A.; Turner-Evans, D.; Kelzenberg, M. D.; Walter, M. G.; McKone, J. R.; Brunschwig, B. S.; Atwater, H. A.; Lewis, N. S. Photoelectrochemical Hydrogen Evolution Using Si Microwire Arrays. *J. Am. Chem. Soc.* **2011**, *133* (5), 1216–1219.

(19) Seger, B.; Pedersen, T.; Laursen, A. B.; Vesborg, P. C. K.; Hansen, O.; Chorkendorff, I. Using TiO2 as a Conductive Protective Layer for Photocathodic H2 Evolution. *J. Am. Chem. Soc.* **2013**, *135* (3), 1057–1064.

(20) Minggu, L. J.; Wan Daud, W. R.; Kassim, M. B. An Overview of Photocells and Photoreactors for Photoelectrochemical Water Splitting. *Int. J. Hydrogen Energy* **2010**, *35* (11), 5233–5244.

(21) McKone, J. R.; Lewis, N. S.; Gray, H. B. Will Solar-Driven Water-Splitting Devices See the Light of Day? *Chem. Mater.* **2014**, *26* (1), 407–414.

(22) Bae, D.; Shayestehaminzadeh, S.; Thorsteinsson, E. B.; Pedersen, T.; Hansen, O.; Seger, B.; Vesborg, P. C. K.; Ólafsson, S.; Chorkendorff, I. Protection of Si Photocathode Using TiO2 Deposited by High Power Impulse Magnetron Sputtering for H2 Evolution in Alkaline Media. *Sol. Energy Mater. Sol. Cells* **2016**, *144* (JANUARY), 758–765.

(23) Bhola, S. M.; Mishra, B. Effect of Ph on the Electrochemical Properties of Oxides Formed over β - Ti-15Mo and Mixed Ti-6Al-4v Alloys. *Int. J. Electrochem. Sci.* **2013**, *8* (5), 7075–7087.

(24) Kast, M. G.; Enman, L. J.; Gurnon, N. J.; Nadarajah, A.; Boettcher, S. W. Solution-Deposited F:SnO□/TiO□ as a Base-Stable Protective Layer and Antireflective Coating for Microtextured Buried-Junction H□-Evolving Si Photocathodes. *ACS Appl. Mater. Interfaces* **2014**, *6* (24), 22830–22837.

(25) Seger, B.; Tilley, S. D.; Pedersen, T.; Vesborg, P. C. K.; Hansen, O.; Graetzel, M.; Chorkendorff, I. Silicon Protected with Atomic Layer Deposited TiO2: Conducting versus

Tunnelling through TiO2. *J. Mater. Chem. a* **2013**, *1* (47), 15089–15094.

(26) Avasthi, S.; McClain, W. E.; Man, G.; Kahn, A.; Schwartz, J.; Sturm, J. C. Hole-Blocking Titanium-Oxide/silicon Heterojunction and Its Application to Photovoltaics. *Appl. Phys. Lett.* **2013**, *102* (20), 0–4.

(27) Chen, Y. W.; Prange, J. D.; Dühnen, S.; Park, Y.; Gunji, M.; Chidsey, C. E. D.; McIntyre, P. C. Atomic Layer-Deposited Tunnel Oxide Stabilizes Silicon Photoanodes for Water Oxidation. *Nat. Mater.* **2011**, *10* (7), 539–544.

(28) Hu, S.; Shaner, M. R.; Beardslee, J. a; Lichterman, M.; Brunschwig, B. S.; Lewis, N. S. Amorphous TiO□ Coatings Stabilize Si, GaAs, and GaP Photoanodes for Efficient Water Oxidation. *Science* **2014**, *344* (6187), 1005–1009.

(29) Sivula, K. Defects Give New Life to an Old Material: Electronically Leaky Titania as a Photoanode Protection Layer. *ChemCatChem* **2014**, 2796–2797.

(30) McDowell, M. T.; Lichterman, M. F.; Carim, A. I.; Liu, R.; Hu, S.; Brunschwig, B. S.; Lewis, N. S. The Influence of Structure and Processing on the Behavior of TiO_2 Protective Layers for Stabilization of N-Si/TiO_2/Ni Photoanodes for Water Oxidation. *ACS Appl. Mater. Interfaces* **2015**, *7* (28), 15189–15199.

(31) Scheuermann, A. G.; Prange, J. D.; Gunji, M.; Chidsey, C. E. D.; McIntyre, P. C. Effects of Catalyst Material and Atomic Layer Deposited TiO2 Oxide Thickness on the Water Oxidation Performance of Metal–insulator–silicon Anodes. *Energy Environ. Sci.* **2013**, *6* (8), 2487.

(32) Mei, B.; Pedersen, T.; Malacrida, P.; Bae, D.; Frydendal, R.; Hansen, O.; Vesborg, P. C.

K.; Seger, B.; Chorkendorff, I. Crystalline TiO_2: A Generic and Effective Electron-Conducting Protection Layer for Photoanodes and -Cathodes. *J. Phys. Chem. C* **2015**, *119* (27), 15019–15027.

(33) Seger, B.; Tilley, D. S.; Pedersen, T.; Vesborg, P. C. K.; Hansen, O.; Grätzel, M.; Chorkendorff, I. Silicon Protected with Atomic Layer Deposited TiO2: Durability Studies of Photocathodic H2 Evolution. *RSC Adv.* **2013**, *3* (48), 25902–25907.

(34) Paracchino, A.; Laporte, V.; Sivula, K.; Grätzel, M.; Thimsen, E. Highly Active Oxide Photocathode for Photoelectrochemical Water Reduction. *Nat. Mater.* **2011**, *10* (6), 456–461.

(35) Wang, T.; Luo, Z.; Li, C.; Gong, J. Controllable Fabrication of Nanostructured Materials for Photoelectrochemical Water Splitting via Atomic Layer Deposition. *Chem. Soc. Rev.* **2014**, *43* (22), 7469–7484.

(36) Ros, C.; Andreu, T.; Giraldo, S.; Sánchez, Y.; Morante, J. R. Conformal Chalcopyrite Based Photocathode for Solar Refinery Applications. *Sol. Energy Mater. Sol. Cells* **2016**, *158*, 184–188.

(37) Miikkulainen, V.; Leskelä, M.; Ritala, M.; Puurunen, R. L.; Leskelä, M.; Ritala, M.; Puurunen, R. L. Crystallinity of Inorganic Films Grown by Atomic Layer Deposition: Overview and General Trends. *J. Appl. Phys.* **2013**, *113* (2), 21301.

(38) Aarik, J.; Aidla, A.; Uustare, T.; Sammelselg, V. Morphology and Structure of TiO2 Thin Films Grown by Atomic Layer Deposition. *J. Cryst. Growth* **1995**, *148* (3), 268–275.

(39) Li, W.; Ni, C.; Lin, H.; Huang, C. P.; Shah, S. I. Size Dependence of Thermal Stability of

TiO2 Nanoparticles. *J. Appl. Phys.* **2004**, *96* (11), 6663.

(40) Polman, A.; Knight, M.; Garnett, E. C.; Ehrler, B.; Sinke, W. C.; Summary, R.; Polman, A.; Knight, M.; Garnett, E. C.; Ehrler, B.; Sinke, W. C. Photovoltaic Materials – Present Efficiencies and Future Challenges. *Science (80-.).* **2016**, *352* (6283), 307.

(41) Scheuermann, A. G.; Lawrence, J. P.; Kemp, K. W.; Ito, T.; Walsh, A.; Chidsey, C. E. D.; Hurley, P. K.; McIntyre, P. C. Design Principles for Maximizing Photovoltage in Metal-Oxide-Protected Water-Splitting Photoanodes. *Nat. Mater.* **2016**, *15* (October), 99–105.

(42) Das, C.; Kot, M.; Henkel, K.; Schmeisser, D. Engineering of Sub-Nanometer SiOx Thickness in Si Photocathodes for Optimized Open Circuit Potential. *ChemSusChem* **2016**, *9* (17), 2332–2336.

(43) Reiners, M.; Xu, K.; Aslam, N.; Devi, A.; Waser, R.; Hoffmann-Eifert, S. Growth and Crystallization of TiO 2 Thin Films by Atomic Layer Deposition Using a Novel Amido Guanidinate Titanium Source and Tetrakis-Dimethylamido-Titanium. *Chem. Mater.* **2013**, *25* (15), 2934–2943.

(44) Aarik, J.; Kasikov, A.; Niilisk, A. Spectrophotometric and Raman Spectroscopic Characterization of ALD Grown TiO2 Thin Films. *Proc. SPIE* **2007**, *6596*, 6596161–6596166.

(45) Puurunen, R. L.; Sajavaara, T.; Santala, E.; Miikkulainen, V.; Saukkonen, T.; Laitinen, M.; Leskelä, M. Controlling the Crystallinity and Roughness of Atomic Layer Deposited Titanium Dioxide Films. *J. Nanosci. Nanotechnol.* **2011**, *11* (9), 8101–8107.

(46) Yang, X.; Liu, R.; Lei, Y.; Li, P.; Wang, K.; Zheng, Z.; Wang, D. Dual Influence of

Reduction Annealing on Diffused Hematite/FTO Junction for Enhanced Photoelectrochemical Water Oxidation. *ACS Appl. Mater. Interfaces* **2016**, *8* (25), 16476–16485.

(47) Tang, Z.; Fang, L.; Xu, N.; Liu, R. Forming Compliance Dominated Memristive Switching through Interfacial Reaction in Ti/TiO2/Au Structure. *J. Appl. Phys.* **2015**, *118* (185309), 1–5.

(48) Salaoru, I.; Khiat, A.; Li, Q.; Berdan, R.; Prodromakis, T. Pulse-Induced Resistive and Capacitive Switching in TiO2 Thin Film Devices. *Appl. Phys. Lett.* **2013**, *103* (233513), 1–4.

(49) Jeong, D. S.; Schroeder, H.; Waser, R. Impedance Spectroscopy of TiO2 Thin Films Showing Resistive Switching. *Appl. Phys. Lett.* **2006**, *89* (8), 1–4.

(50) Choi, B. J.; Jeong, D. S.; Kim, S. K.; Rohde, C.; Choi, S.; Oh, J. H.; Kim, H. J.; Hwang, C. S.; Szot, K.; Waser, R.; Reichenberg, B.; Tiedke, S. Resistive Switching Mechanism of TiO 2 Thin Films Grown by Atomic-Layer Deposition. *J. Appl. Phys.* **2005**, *98* (3), 1–10.

(51) Bousoulas, P.; Michelakaki, I.; Tsoukalas, D. Influence of Ti Top Electrode Thickness on the Resistive Switching Properties of Forming Free and Self-Rectified TiO2 - X Thin Films. *Thin Solid Films* **2014**, *571* (P1), 23–31.

(52) Chiu, F. A Review on Conduction Mechanisms in Dielectric Films. *Adv. Mater. Sci. Eng.* **2014**, *2014*, 1–18.

(53) Sheng, W.; Gasteiger, H. A.; Shao-Horn, Y. Hydrogen Oxidation and Evolution Reaction Kinetics on Platinum: Acid vs Alkaline Electrolytes. *J. Electrochem. Soc.* **2010**, *157* (11),

B1529.

TOC GRAPHIC

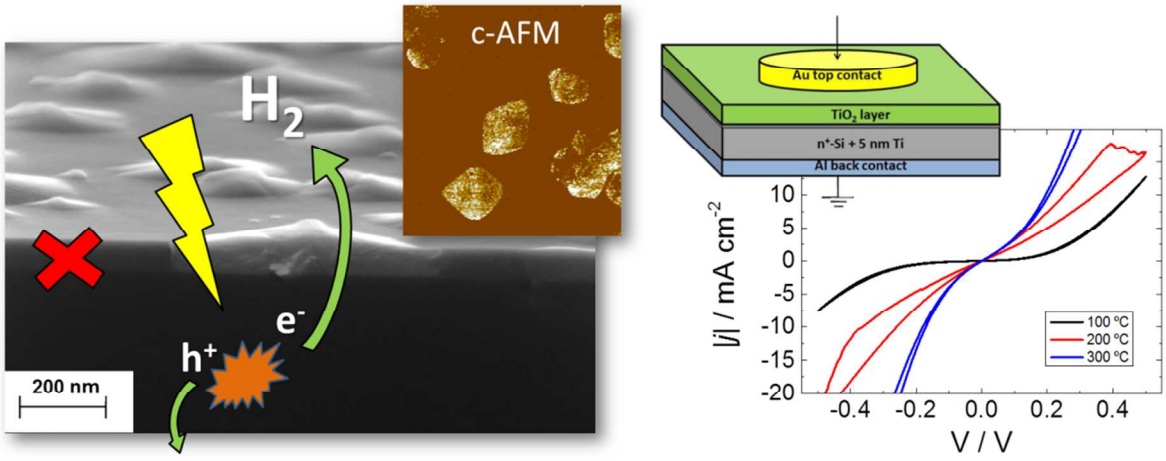
c-AFM
H2
e-
h+
200 nm
Au top contact
TiO2 layer
n+-Si + 5 nm Ti
Al back contact
|j| / mA cm-2
10
5
0
-5
-10
-15
-20
-0.4
-0.2
0.0
0.2
0.4
V / V
100 °C
200 °C
300 °C